Minimum Mass Design of Large-Scale Space Trusses Subjected to Thermal Gradients

R. Brett Williams, Ph.D.* and Gregory. S. Agnes, Ph.D.†
Jet Propulsion Laboratory, California Institute of Technology, Pasadena, CA, 91109

Lightweight, deployable trusses are commonly used to support space-borne instruments including RF reflectors, radar panels, and telescope optics. While in orbit, these support structures are subjected to thermal gradients that vary with altitude, location in orbit, and self-shadowing. Since these instruments have tight dimensional-stability requirements, their truss members are often covered with multi-layer insulation (MLI) blankets to minimize thermal distortions. This paper develops a radiation heat transfer model to predict the thermal gradient experienced by a triangular truss supporting a long, linear radar panel in Medium Earth Orbit (MEO). The influence of self-shadowing effects of the radar panel are included in the analysis, and the influence of both MLI thickness and outer covers/coatings on the magnitude of the thermal gradient are formed into a simple, two-dimensional analysis. This thermal model is then used to size and estimate the structural mass of a triangular truss that meets a given set of structural requirements.

Nomenclature

A_b = Area of batten strut
A_d = Area of diagonal strut
A_l = Area of longeron strut
AF = Albedo factor
a = Length of truss bay
α = coefficient of thermal expansion
α^s = Solar absorptivity
b = Length of truss batten
β = Orbital angle
β_d = Factor relating A_d to A_l
β_b = Factor relating A_b to A_l
c = Specific heat
ΔT = Temperature gradient
δ = Thermal distortion
E = Modulus of elasticity
ε = Emissivity
ε^* = Effective emissivity of MLI blanket
F = View factor
f = Natural frequency
g = Acceleration due to gravity
H = Height of truss
I = Moment of inertia of truss
L = Total truss length
M = Total system mass
m = Mass of a thermal node
Q_d = Heat generated by radar electronics

* Member of Technical Staff, Advanced Deployable Structures Group, MS 299-101, AIAA Member, rowilli6@jpl.nasa.gov
† Group Leader, Precision Deployable Structures Group, MS 299-101, Senior AIAA Member.

q = Heat flow per unit area
θ = Angle of albedo reflection
r = Radius of circular orbit
r_l = Radius of longeron
R = Radius of earth
R = Radius of truss
ρ = Volume density of graphite epoxy composite
ρ_{MLI} = Volume density of MLI blankets
σ = Stefan-Boltzmann constant
T = Absolute temperature
t = Time
t = Wall thickness of tube longeron
t_{MLI} = MLI blanket thickness
τ = Angle between orbital plane and terminator
V_s = Orbital velocity
ψ = Angle btw. solar vector and surface normal

Subscripts:
s = Solar
e = Earth
a = Albedo
1 = Node 1 – front longerons
4 = Node 4 – back longeron
p = Radar panel
oc = Outer cover
t = Tube
β = Beta cloth

I. Introduction

Increased science requirements for space-based instruments over the past few decades have amplified the need for large-scale support structures that are not only deployable, but also low in mass. Popular applications such as optical and RF reflectors and membrane antennae demand high-precision structural components to meet stringent flatness requirements. While thermal deformations are neglected for many satellites, designs for these precision structures must include such effects, which are proportional to material thermal properties and bulk temperature change. Since material properties are difficult to alter, thermal blankets (also known as multi-layer insulation (MLI)) are often added to key structural components to minimize temperature variations. While this added insulation is effective, it imposes a mass penalty on the structure.

There are many spacecraft missions in the concept or development phase that will require structural hardware that is on the scale of up to hundreds of meters, with potentially larger structures in the future. Examples of these large structures, which are typically subjected to small bending, compressive, or torsional loads, include solar sails, sunshades, and large aperture reflectors. Such large assemblies will have to be as light as possible, thus requiring long, slender structural members. A seminal paper in the field of large scale, light weight space structures is by Mikulus[3]. This paper calculates the structural masses for the thin-walled tubes, isogrid tubes, and tubular and solid rod columns as a function of applied load. The failure criteria used is based on the expected buckling modes for, in particular, long, lightly loaded structures. The influence of imperfections, such as thermal gradients, manufacturing, and lateral accelerations, is addressed as well. Much of the structural and mass analysis and requirements presented in this report were also presented by Mikulas in an ISAT report[2]. Mahaney and Strode present a thermal analysis of a bare flat or parabolic truss in various earth orbits[3], where as earth IR heating[4] and albedo heating[5] are covered in more detail in other publications. The thermal modeling[6], construction[7], and properties[7, 8] of MLI blankets are covered in popular space mission design handbooks.

This report begins by defining the geometry and summarizing the structural analysis required for the triangular support truss with the thin-walled circular tube longerons of interest[9]. Mechanical requirements and equations used to estimate both the bare and insulated truss masses are presented[9], followed by an orbital and radiation heat load analysis for the desired mission. The effects of these environmental loads on the temperature response of the truss and the radar panel it supports are then considered, first for a bare graphite-epoxy truss, then for the truss with a

variety of MLI blanket thicknesses and outer coverings. Based on the thermal gradient present across the various truss configurations, the structural requirements are used to size and then estimate their masses and identify the minimum-mass design.

II. Description of Truss

This section will introduce the triangular truss under consideration in this paper. The geometry and material properties will be presented, followed by basic equations that are used to analyze various types of mechanical behavior, such as thermal distortion and vibration characteristics.

A. Triangular Truss Definition

This paper considers the analysis of a single laced triangular truss with one double laced side. The double laced side is the one presumed to support a reflector panel, as seen on the bottom of the truss in Figure 1a. This truss, having a total length *L,* is depicted as having only three bays, however, the total truss is composed of *n* bays, each having length *a*. The reflector panel is assumed to be an L-band radar reflector that is 100 m long by 2 m wide and having an areal density of 10 kg/m^2. The mass of the reflector, as well as the spacecraft mass (taken to be 1000 kg) is assumed to be uniformly distributed for this preliminary investigation. The truss joints are assumed to behave in a pin-like manner. The cross section geometry of the triangular truss is shown in Figure 1b.

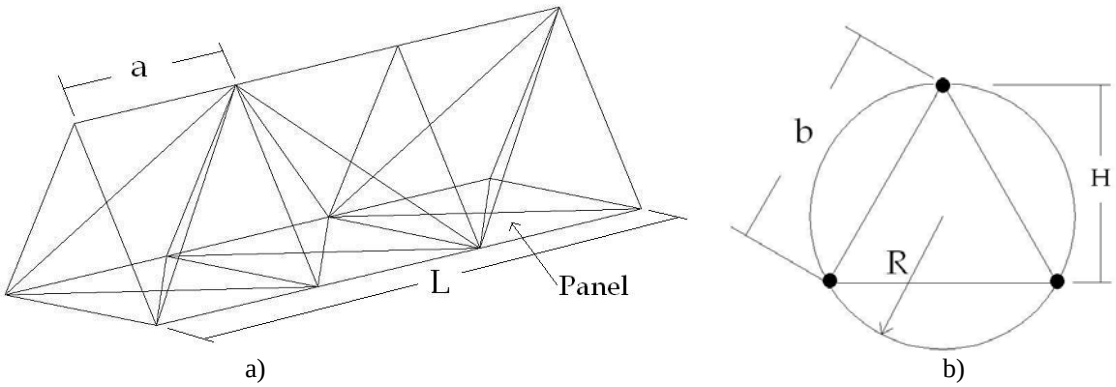

Figure 1: Triangular truss definitions: a) 3D View of Truss, b) End View of Truss and Longerons.

For this study, the three longerons in this truss are considered to be thin-walled tubes as shown in Figure 2.

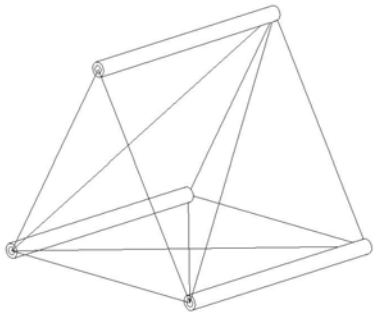

Figure 2: One Bay of a Tubular Longeron Truss.

B. Truss Geometry and Material Properties

For the analysis of a triangular truss, a few formulae for the geometry and stiffness properties are required. The radius of the truss, defined in Figure 1b is[2]

$$R = \frac{b}{\sqrt{3}} \tag{1}$$

while the height *H* of the truss is given by

$$H = \frac{b\sqrt{3}}{2} \tag{2}$$

The moment of inertia about the centroid of the truss cross section is

$$I = b^2 \frac{A_l}{2} \tag{3}$$

where A_l is the cross sectional area of a single longeron. For a thin-walled tube longeron with radius r and wall thickness t, then the area is given as

$$A_l = 2\pi r_l t_l \tag{4}$$

The geometry of the battens and diagonals is not investigated in detail, but rather, taken to be proportional to the area of the longerons[2], such that

$$A_d = \beta_d A_l \quad and \quad A_b = \beta_b A_l \tag{5}$$

In Eq. 5, A represents cross sectional area, β is a scaling factor, and the subscripts b, d, and l refer to batten, diagonal, and longeron struts, respectively.

All members of the trusses under consideration are assumed to be made from a graphite-epoxy composite material having quasi-isotropic in-plane material properties. To minimize thermal loading on the truss, MLI blankets can be added, which add a non-structural mass penalty. The required geometric and material properties for both the graphite epoxy and the MLI blankets are given in Table 1[2,6].

Table 1: Material and Geometric Properties

Property	Value	Units
E	50	GPa
ρ	1522	kg/m^3
α	1E-06	m/m/C
δ	0.012	m
ρ_{MLI}	249	kg/m^3
L	100	m
f	0.1	Hz
β_b	0.5	-
β_d	0.25	-
t_l	5.08E-04	m
t_{MLI}	0.003	m
Mpanel	2000	kg
Mspacecraft	1000	kg

C. Mechanical Requirements for Truss

This section presents a few formulae which are used to design the truss to meet various geometric and structural response requirements. The first requirement for the truss is that its longeron members may not be too slender. That is, it is very difficult to manufacture an extremely long, thin rod or thin-walled tube that has negligible straightness imperfections. Thus, a limit on the slenderness ratio for all of the longerons to be considered is

$$\frac{a}{2r_l} \le 100 \tag{6}$$

This requirement restricts the length to diameter ratio of a longeron member to be less than or equal to 100. Next, the truss should have some minimum natural frequency to minimize vibrational disturbances while on-orbit. The first natural frequency of flexural vibration for a free-free beam with total mass *M*, length *L*, modulus of elasticity *E* and moment of inertia given by Eq. 3 is[2]

$$f = \frac{22.4}{2\pi}\sqrt{\frac{EI}{ML^3}} \tag{7}$$

Lastly, the truss must meet a specification on how much it can warp in the presence of a thermal gradient. Thus, for a truss subjected to a temperature gradient between its front and back longerons, ΔT, the thermal distortion depicted in Figure 3 is calculated as[2]

$$\delta = \frac{2\alpha\,\Delta T\,L^2}{8b\sqrt{3}} \tag{8}$$

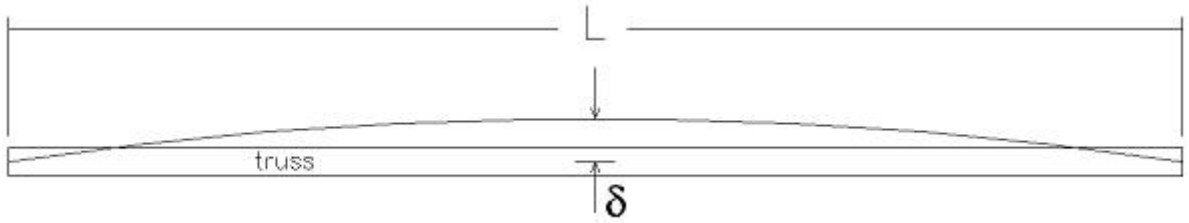

Figure 3: Thermal Distortion Resulting from Temperature Gradient.

D. Mass Calculations

For the triangular trusses shown in Figure 2 with a large number of bays *n*, the total mass of the truss is[2]

$$M_{truss} = LA_l\rho\left(3 + 4\sqrt{2}\beta_d + 3\beta_b\right) \tag{9}$$

If these truss members are covered with MLI, as shown in Figure 4, the total mass of the insulation blankets is

$$M_{MLI} = 2\pi L\,\rho_{MLI}t_{MLI}\left(3\left(r_l + \frac{t_{MLI}}{2}\right) + 4\sqrt{2}\left(\beta_d r_l + \frac{t_{MLI}}{2}\right) + 3\left(\beta_b r_l + \frac{t_{MLI}}{2}\right)\right) \tag{10}$$

where *r* is the radius of the longeron and t_{MLI} is the thickness of the MLI blanket.

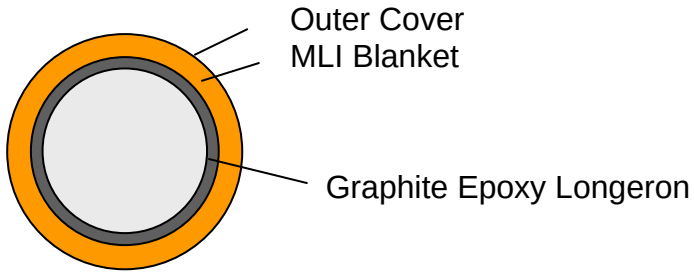

Figure 4: Cross-Section of Longeron Covered with MLI Blanket and Outer Cover

Equation 10 can be used to calculate both the mass of the MLI and the outer cover (OC). Thus the total system mass is

$$M = M_{panel} + M_{spacecraft} + M_{truss} + M_{MLI} + M_{OC} \tag{11}$$

III. Thermal Analysis

The radar panel supported by the truss described above is designed to orbit the earth; therefore the thermal loading on the truss will change as a function of the type of orbit, position in orbit, and orbit altitude.

A. Orbital Analysis

Figure 5 shows the example orbit used in this paper, looking down on the North Pole. The truss resides in a circular MEO orbit (10,000 km altitude) in the equatorial plane, and the radar panel is always nadir-pointed while the long axis of the truss is parallel to the velocity vector. For this orbit, the velocity is given by

$$V_s = \sqrt{\frac{gR_e^2}{r}} \tag{12}$$

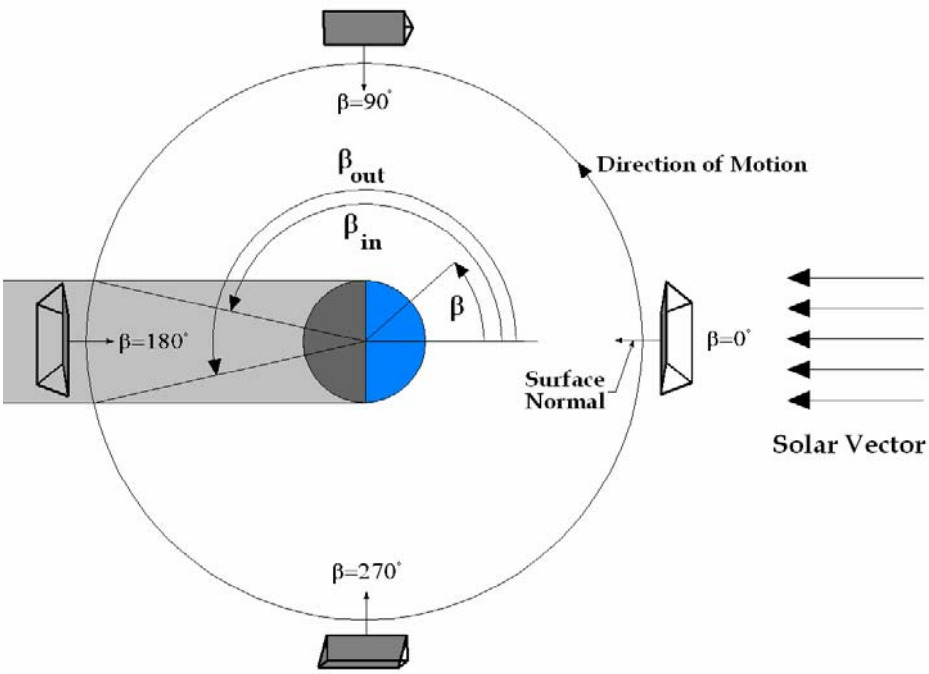

Figure 5: Top View of Truss in Circular, Earth-Facing Equatorial Orbit.

where R is the radius of the earth (6378 km), r is the radius of the circular orbit (16378 km), and g is the acceleration of gravity (9.81 m/s^2). The orbital period is then

$$t = \frac{2\pi r}{V_s} \tag{13}$$

It has been shown that the truss will enter the earths shadow at an angle of[3]

$$\beta_{in} = \sin^{-1}\left(\frac{\sin\left(\cos^{-1}\frac{R_e}{r}\right)}{\sin\tau}\right) + \frac{\pi}{2} \tag{14}$$

which occurs at time

$$t_{in} = \frac{t\,\beta_{in}}{2\pi} \tag{15}$$

The time spent in the shadow is

$$t_s = \frac{\pi r}{V_s}\left(1 - \frac{2}{\pi}\sin^{-1}\left(\frac{\sin\left(\cos^{-1}\frac{R_e}{r}\right)}{\sin\tau}\right)\right) \tag{16}$$

where the angle between the orbital plane and the terminator line, τ, is 90° for an equatorial orbit. Therefore, the truss exits the shadow of the earth at

$$t_{out} = t_{in} + t_s \tag{17}$$

B. Thermal Loads

This section defines the three main sources of external thermal loads that act on the truss, solar, earth IR, and earth albedo. The solar heating incident upon the truss is

$$q_s = 1390\left(\frac{W}{m^2}\right)\cos\psi \tag{18}$$

It should be noted that the amount of this heat absorbed by the truss members is reduced by the solar absorptivity of the surface, α_s, as seen in the radiation balance analysis that follows. Here, ψ is the angle between the solar flux vector and the surface normal. For the orbit under consideration,

$$\psi = \begin{cases} \beta & \beta \le \dfrac{\pi}{2} \\ \pi - \beta & \dfrac{\pi}{2} < \beta \le \pi \\ \beta - \pi & \pi < \beta \le \dfrac{3\pi}{2} \\ 2\pi - \beta & \dfrac{3\pi}{2} < \beta \le 2\pi \end{cases} \tag{19}$$

The earth is presumed to radiate heat as a black body with at temperature T_e = 250 K, so the portion of this heat that is incident upon the truss member is

$$q_e = \sigma T_e^{\,4} F \tag{20}$$

where σ is the Stefan-Boltzmann constant (5.67x10^{-8} W/m^{2}K^4), and F is the view factor of the earth to the member. For the given truss configuration,

$$F = \frac{\cos\lambda}{H^2} \tag{21}$$

where λ is the angle between the surface normal and the earth heat flux (0° for this study) and $H = r/R$. The amount of heat absorbed by the truss member is reduced by the absorptivity of the truss material to earth radiation. However, for the wavelength of energy the emitted from the earth, the truss is assumed to behave as a gray body, for which the absorptivity and emissivities are equal. Thus, it is equivalent to say that the heat absorbed from earth IR is reduced by the emissivity of the truss member. Next, the heat incident upon the truss from earth albedo is

$$q_a = 1390\left(\frac{W}{m^2}\right) AF\cos\theta F \tag{22}$$

where AF is the fraction of the incident solar radiation reflected (taken to be 0.36[3]), F is the same as in Equation 21, and θ is the reflection angle of the incident solar radiation. For this study, θ is related to the orbital position β by

$$\theta = \begin{cases} \beta & \beta \le \frac{\pi}{2} \\ \frac{\pi}{2} & \frac{\pi}{2} < \beta \le \frac{3\pi}{2} \\ 2\pi - \beta & \frac{3\pi}{2} < \beta \le 2\pi \end{cases} \tag{23}$$

The actual amount of albedo heating absorbed by the truss member is reduced by the absorptivity of the truss member. Since albedo is reflected solar radiation, it is assumed that the absorptivity to earth albedo is equal to the solar absorptivity.

C. Shadowing Effects

In the earth-facing, equatorial orbit described in Figure 5, the thermal loads defined above heat parts of the truss differently. The main source of heat in earth orbit is from the sun, which is defined in Equation 18 and plotted in Figure 6 for the various truss components of interest. The time spent in the earth's shadow is determined from Equation 16.

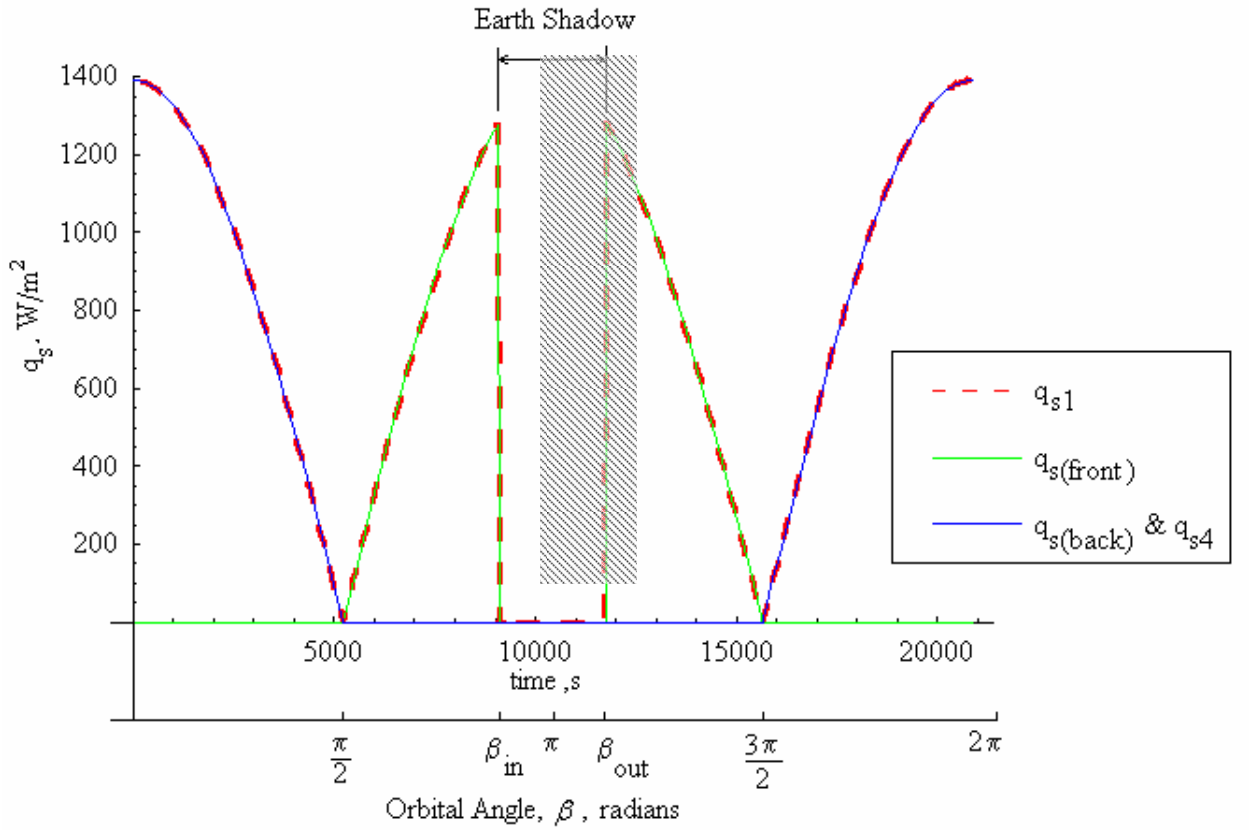

Figure 6: Incident Solar Heat for Front Longeron (1), Front of Panel, Back of Panel and Back Longeron (4)

Clearly, while in the shadow of the earth, the entire truss is blocked from solar heating. The two front (earth facing) longerons (denoted 1) always see heat from the sun (except when in the earth shadow), as well as earth IR, and earth albedo while on the sunny side of the planet. The front of the radar panel is always exposed to earth IR and earth albedo (on the daytime side of the planet), but not to solar heating on the daytime side of the planet. Conversely, the back of the radar panel sees the sun only during the daytime. While the radar panel prevents the back tube from ever being exposed to earth IR or albedo at any point in the orbit, the panel does exchange heat with the back tube directly. Furthermore, the radar panel shadows the back tube from solar heating when β is between 90° and 270°.

D. Radiation Analysis and Temperature Response

From the environmental loading and shadowing effects described above, radiation balance equations can be derived for the front longerons, which are thermally identical and not coupled to any other structural members, and the radar panel and rear longeron, whose temperatures are coupled. In order to establish a temperature baseline, the truss longerons will be considered bare graphite-epoxy, and then various types and amounts of insulation blankets will be applied.

1. Bare Longerons

Figure 7 shows the front longeron of the truss and the associated heat flows. Since heat exchange between truss members and conduction between the radar panel and truss members is ignored, the front longeron is thermally uncoupled from the rest of the structure and may be considered independently.

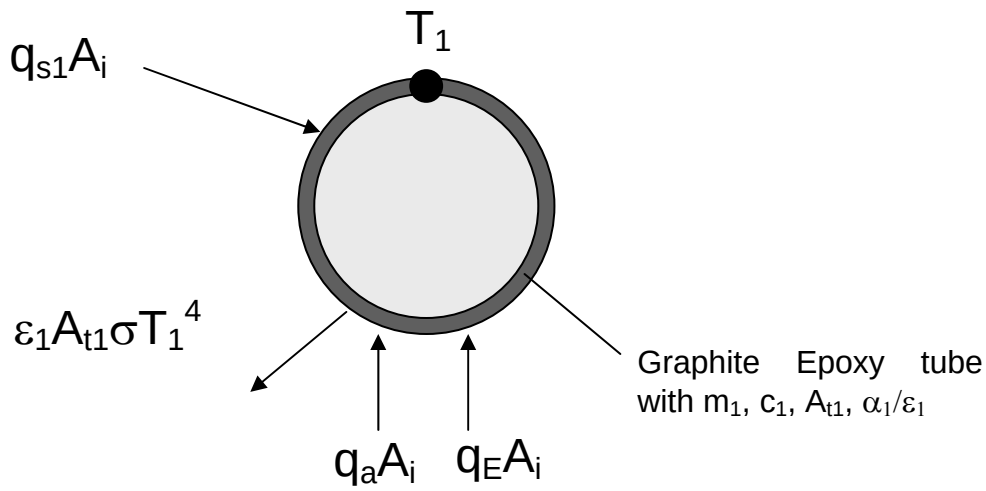

Figure 7: Heats Flows on the Bare Front Longeron.

An energy balance on the front longeron (node 1) yields

$$m_1 c_1 \frac{dT_1}{dt} = \alpha_1^s A_i \left(q_{s1} + q_a\right) + \varepsilon_1 A_i q_E - \varepsilon_1 \sigma T_1^4 A_{t1} \tag{24}$$

where the m is the mass, c is the specific heat, T is the temperature, A_i is the incident (projected) area, and A_t is the radiative (surface) area of the tube, α is the solar absorptivity, ε is the emissivity, and the various q are defined above.

Next, the radar panel and back longeron are considered. Since the back longeron sees a significant portion of and exchanges heat with the radar panel, these two components are thermally coupled and must be considered together as a system, shown in Figure 8. The backside of the radar panel is assumed to be covered with 20 layer MLI blankets whose Kapton outer cover is painted white, while the front side is covered with RF-transparent beta cloth, which is provides better thermal properties than the bare radar electronics cells. This panel configuration is assumed to remain unchanged regardless of the type of insulation or coatings applied to the longerons. In this system, there are three nodes whose temperatures are of interest: the panel (T_p), the outer cover (OC) of the panel MLI (T_{ocp}), and the back longeron (T_4). The beta cloth is assumed to be at the same temperature as radar panel. The thermal mass of the MLI blanket is lumped into the mass of the panel. A radiation balance on the back longeron (node 4) yields

$$m_4 c_4 \frac{dT_4}{dt} = \alpha_4^s A_i q_s + F_{4-p} A_{t4} \varepsilon_4 \varepsilon_{ocp} \left(\sigma T_{ocp}^4 - \sigma T_4^4\right) - F_{4-space} \varepsilon_4 A_{t4} \sigma T_4^4 \tag{25}$$

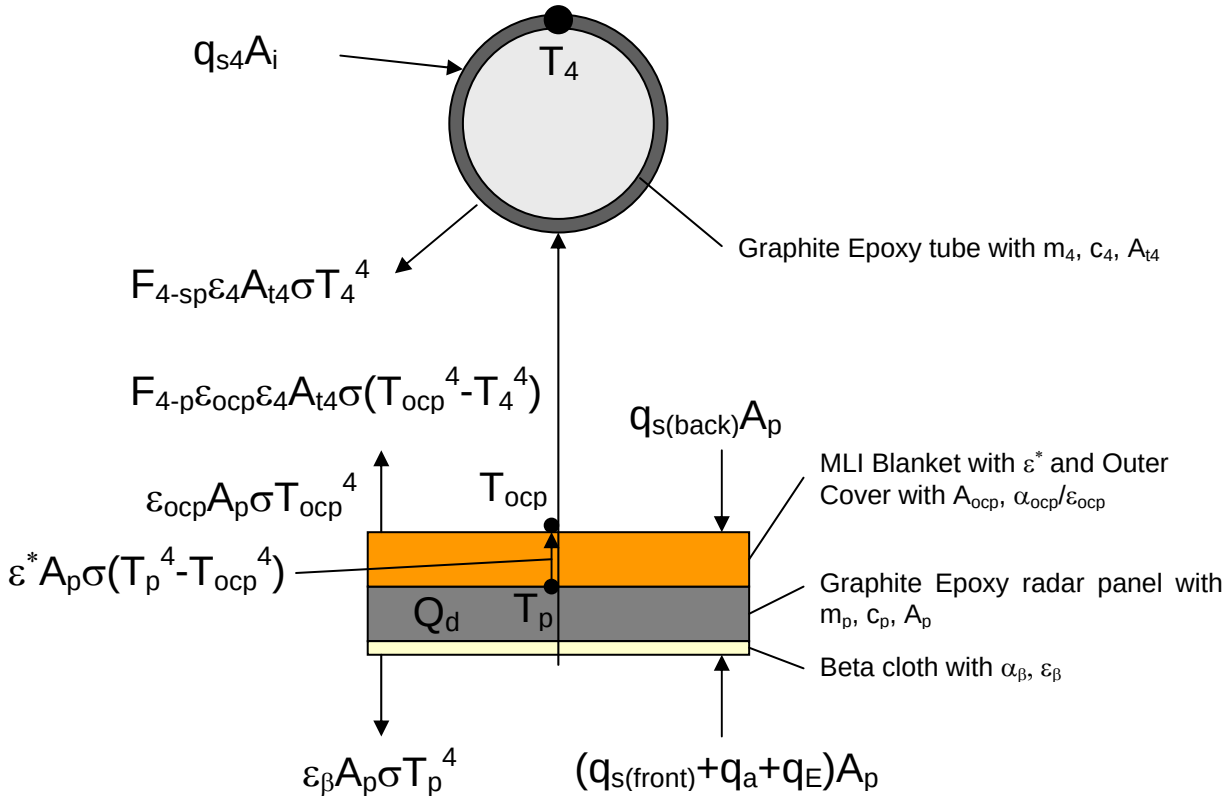

Figure 8: Heat Flows on the Coupled, Radar Panel-Bare Rear Longeron

Here, $F_{4\text{-}p}$ is the view factor from the longeron to the panel, and $F_{4\text{-}space}$ is the view factor from the longeron to deep space. Since the panel is considered infinitely long with respect to its width and truss cross-section is an equilateral triangle, $F_{4\text{-}p}$ is taken to be 1/6, while $F_{4\text{-}space}$ is taken to be 5/6. The radiation balance on the outer cover (OC) of the MLI blanket gives

$$m_{oc4}c_{oc4}\frac{dT_{oc4}}{dt} = \alpha_{ocp}^{s}A_p q_{s(back)} + \varepsilon_p^* A_p\left(\sigma T_p^4 - \sigma T_{ocp}^4\right) - \varepsilon_{ocp}A_p\sigma T_{ocp}^4 - A_{t4}F_{4-panel}\varepsilon_4\varepsilon_{ocp}\left(\sigma T_{ocp}^4 - \sigma T_4^4\right) \tag{26}$$

where ε_p^* is the effective emissivity of the MLI, A_p is the area of the panel, and $q_{s(back)}$ is the solar heat incident upon the outer cover of the MLI on the back of the panel resulting from the earth-facing orbit and shadowing effects described above. The radiation balance for the radar panel gives

$$m_p c_p\frac{dT_p}{dt} = Q_d + \alpha_\beta^s A_p\left(q_{s(\,front)} + q_a\right) + \varepsilon_\beta A_p q_E - \varepsilon_p^* A_p\left(\sigma T_p^4 - \sigma T_{ocp}^4\right) - \varepsilon_\beta A_p\sigma T_p^4 \tag{27}$$

where Q_d is the heat dissipated from the radar electronics when they are operational (taken to be 100 W/m^2) and $q_{s(front)}$ is the solar heat incident upon the beta cloth on the front of the radar panel.

Now, Equation 24 for the front longeron and the system of three coupled differential equations (25-27) for the panel and back longeron are solved numerically with the necessary properties from Table 2 to determine the temperature of the various truss components throughout the described orbit. The results are plotted for many orbits to ensure that the temperature variations have reached a steady state response. The temperature responses of the radar panel and the outer cover of its MLI blanket in the "on" and "off" positions are shown in Figure 9.

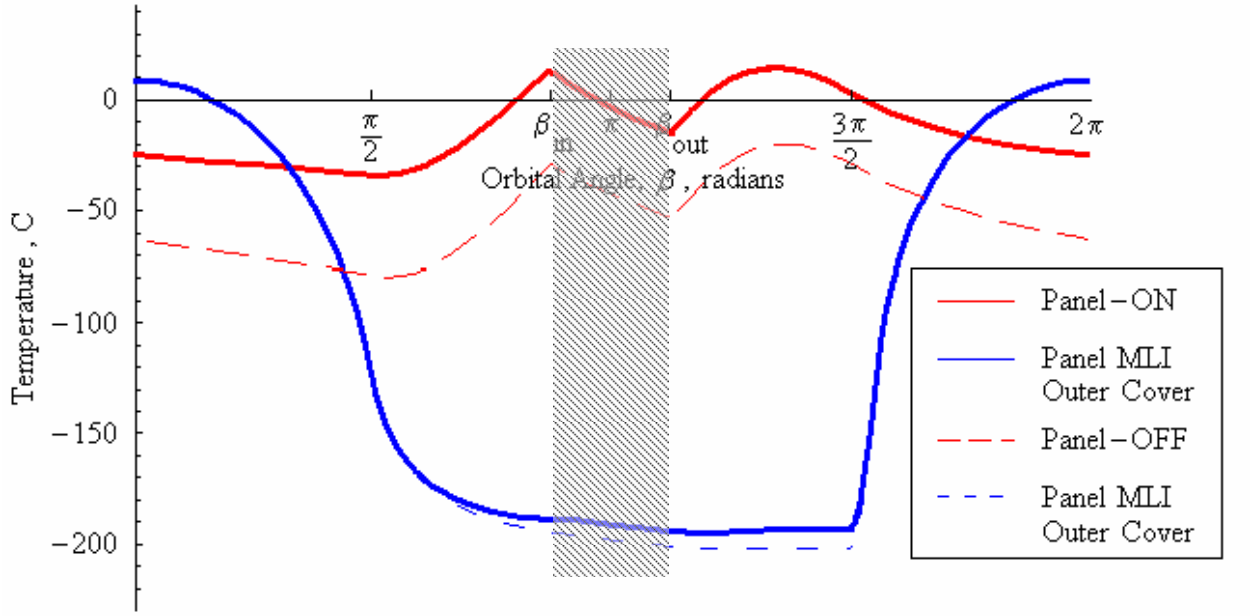

Figure 9: Temperature Response of the Operating Radar Panel and Outer Cover of MLI Blanket

Figure 9 indicates that when the radar panel is powered on, its temperature remains within the operational temperature range for electronics in space (-50°C to 50°C). While the radar panel is off, its temperature also remains within the survivability temperature range (-100°C to 100°C). Additionally, the MLI on the backside of the panel gets quite cold, but such behavior is desired from an insulation blanket. The operational state of the panel does not change the temperature of the MLI outer cover significantly, which means that the heat exchange with the back longeron will not depend strongly on whether the radar is powered on. For this reason, the remainder of the analyses will consider the radar panel in the "on" position.

Figure 10 shows the temperature response of the front and back bare longerons obtained from the numerical solution of Equation 24 and Equations 25-27 with properties from Table 2, as well as the thermal gradient across the truss ($\Delta T = T_{front}-T_{back}$). It is this thermal gradient that is of key interest for this study, as it drives the thermal distortion of the radar panel that must be kept below a specified maximum value. Since the longerons are not insulated, they gain and lose heat quickly, and remain cold throughout the orbit. Since the back longeron only sees the back of the radar panel and occasional sun, it gets very cold, while the front tube is heated by the earth and sun more often and maintains higher temperatures. However, the difference between these two temperature profiles gives the most important information from a thermal distortion point of view. For the worst case, just after the truss exits the earth's shadow, the front longerons are quickly heated by the sun while the back longeron remains shaded by the panel and continues to cool. This shadowing creates a very large maximum ΔT of about 200°C, which, from Equations 2 and 8, would require a truss depth in excess of 20 m, which is not practical this type of linear radar panel backing truss in terms of mass and launch stowage requirements.

One option to lower the magnitude of this thermal gradient is to paint the bare longerons white. In this case, the thermal response of the front and back longerons is given in Figure 11, again obtained from the numerical solution of Equations 24-27 with material properties from Table 2. Since the absorptivity of white paint is much lower than graphite-epoxy, the longerons absorb less heat and are both at lower temperatures throughout the orbit. However, the magnitude of the thermal gradient has been reduced to slightly over 100°C. Such a thermal gradient would still require over 10 m of truss depth, which is still considered excessive for a structure designed to support a 2 m x 100 m long radar panel.

2. Insulated Truss

In the previous section, bare graphite-epoxy or white-painted longerons were found to have a large thermal gradient that required too deep of a supporting truss. In this section, various amounts of MLI blanketing with various outer covers will be applied to the front and back longerons in order to minimize the thermal gradient between them. The addition of MLI blankets to the longerons requires adding a thermal node to their respective models to represent the outer cover. The outer cover has its own thermal response and mass, which can store heat.

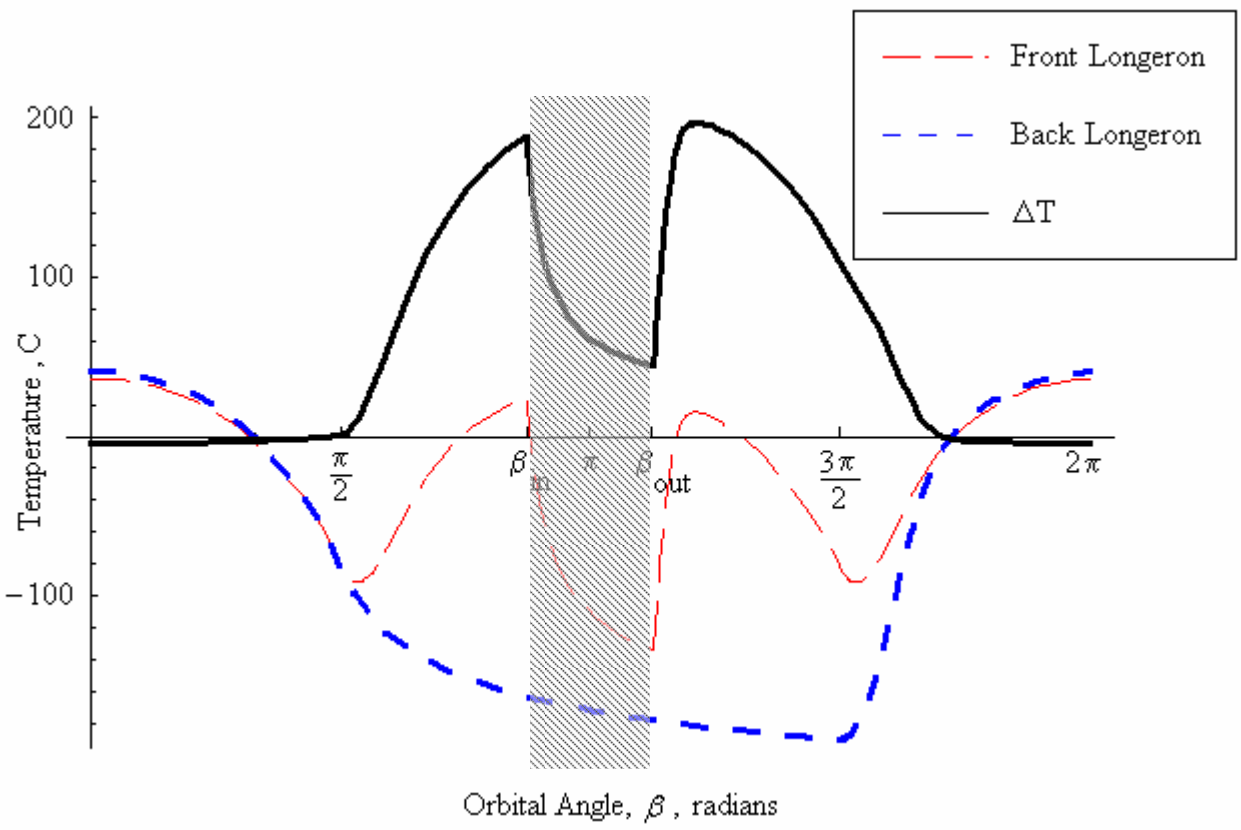

Figure 10: Temperature Response of Bare Front and Back Longerons, and Truss Thermal Gradient.

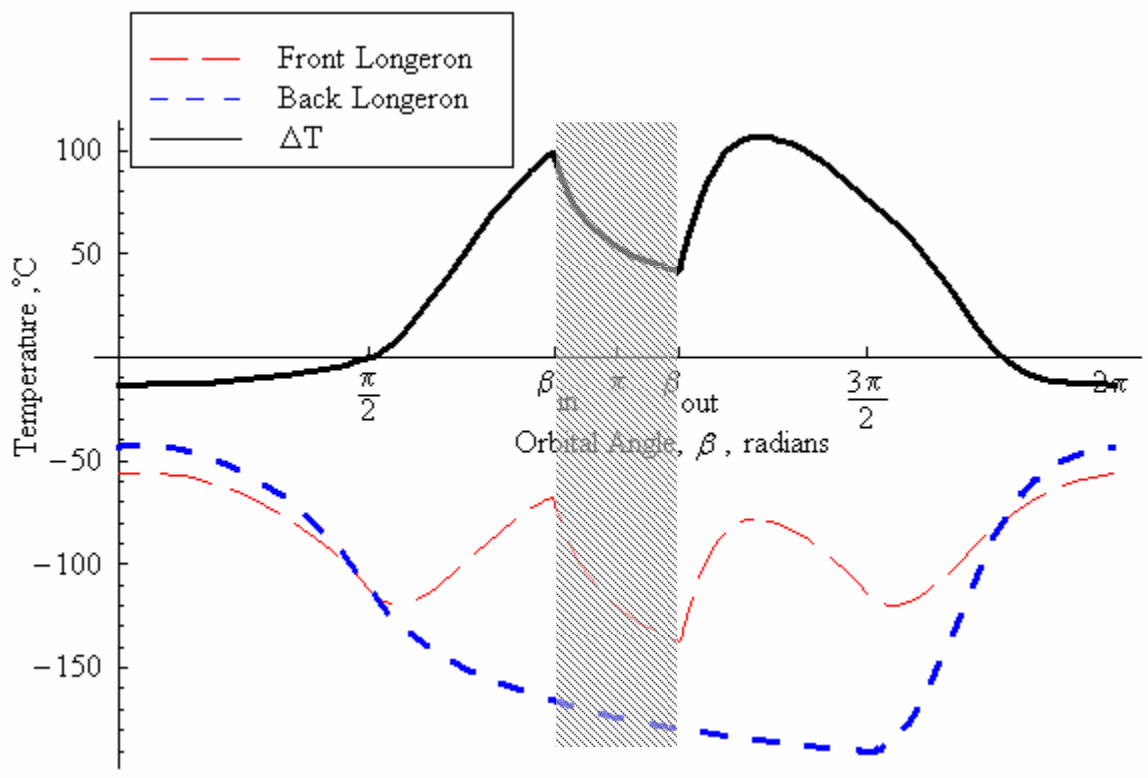

Figure 11: Temperature Response of White-Painted Longerons, and Truss Thermal Gradient.

Figure 12 shows an insulated front longeron. Again, since the insulated longeron does not exchange heat with the radar panel or the other longerons, its response is considered independently.

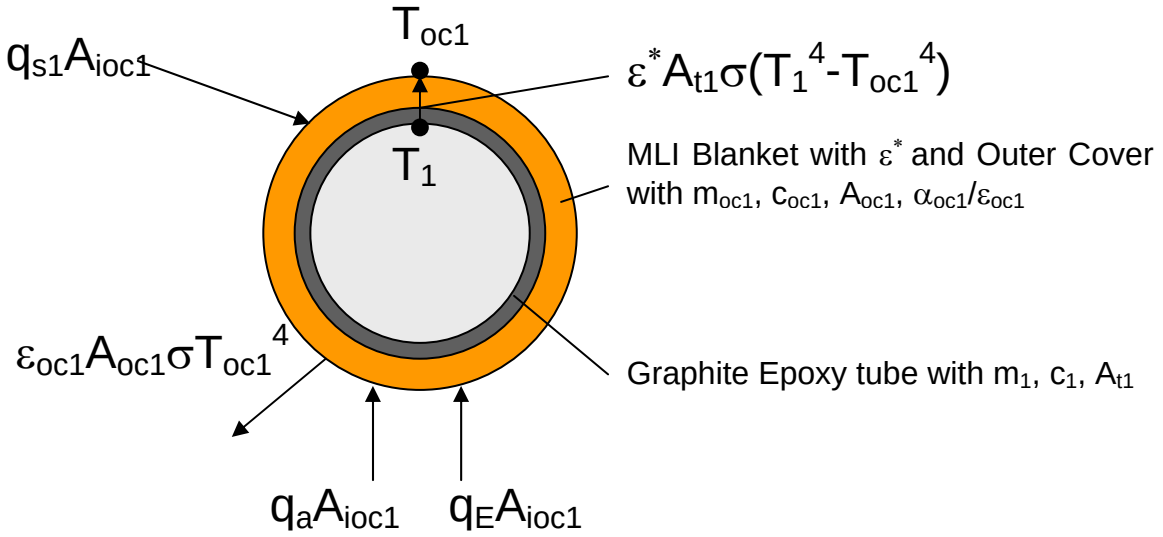

Figure 12: Radiation Heat Flows for Front-Side Longeron Insulated with MLI and Outer Cover (OC).

From Figure 12, the outer cover of the MLI exchanges most of the heat with the space environment, while the only heat transfer for the longeron is radiation exchange with the outer cover though the MLI blanket. A radiation balance on these two nodes gives, for the front longeron

$$m_1 c_1 \frac{dT_1}{dt} = -\varepsilon^*_{tube} A_{t1}\left(\sigma T_1^4 - \sigma T_{oc1}^4\right) \tag{28}$$

and for the front longeron outer cover,

$$m_{oc1} c_{oc1} \frac{dT_{oc1}}{dt} = \alpha_{oc1} A_{ioc1}\left(q_{s1} + q_a\right) + \varepsilon_{oc1} A_{ioc1} q_E + \varepsilon^*_{tube} A_{t1}\left(\sigma T_1^4 - \sigma T_{oc1}^4\right) - \varepsilon_{oc1} A_{oc1}\sigma T_{oc1}^4 \tag{29}$$

For the MLI on the front longeron, ε^* takes a different value than for the MLI on the radar panel. An MLI blanket on a flat surface can achieve a lower effective emissivity than a blanket wrapped around a tube because there is an appreciable amount of heat loss through the seam required on the tube. Next, the radar panel and back longeron are considered. Again, these two components are thermally coupled and must be considered together as a system, shown in Figure 13. The radar panel is insulated as described previously. In this system, there are four nodes whose temperatures are of interest: the panel (T_p), the outer cover (OC) of the panel MLI (T_{ocp}), and the back longeron (T_4), and the outer cover of the back longeron MLI (T_{oc1}). The thermal mass of the MLI blankets is lumped into the mass of the structure it is insulating, while the thermal mass of the outer cover is considered independently.

A radiation balance on the insulated back longeron gives

$$m_4 c_4 \frac{dT_4}{dt} = -\varepsilon^*_{tube} A_{t4}\left(\sigma T_4^4 - \sigma T_{oc4}^4\right) \tag{30}$$

and for the outer cover of the back longeron,

$$m_{oc4} c_{oc4} \frac{dT_{oc4}}{dt} = q_s A_{ioc4} + \varepsilon^*_{tube} A_{t4}\left(\sigma T_4^4 - \sigma T_{oc4}^4\right) + A_{oc4} F_{4-panel}\varepsilon_{oc4}\varepsilon_{oc}\left(\sigma T_{oc}^4 - \sigma T_{oc4}^4\right) - F_{4-space}\varepsilon_{oc4} A_{oc4}\sigma T_{oc4}^4 \tag{31}$$

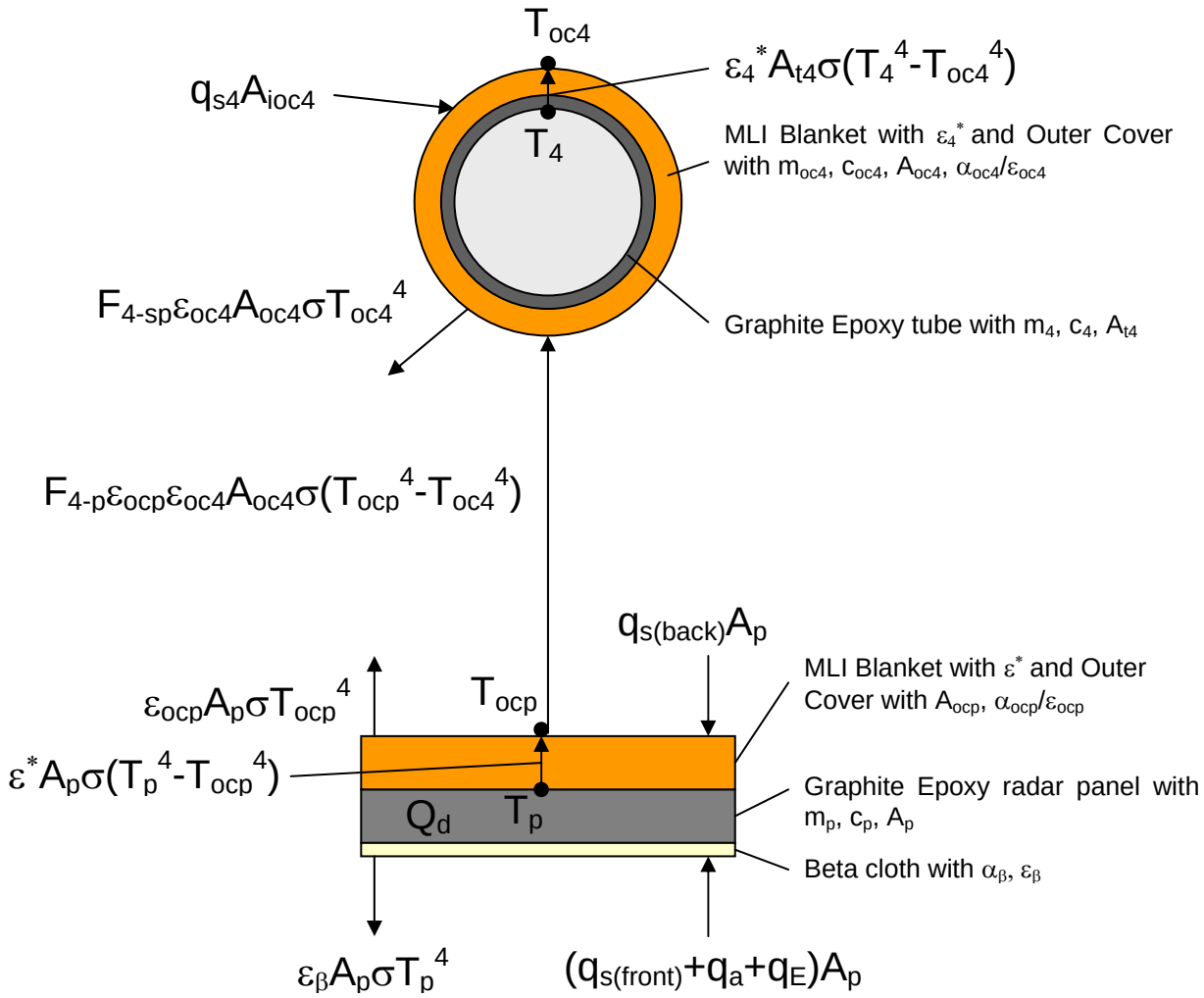

Figure 13: Radiation Heat Flows for Coupled Radar Panel and Back-Side Longeron.

The radiation balance on the radar panel gives

$$m_p c_p \frac{dT_p}{dt} = Q_d - \varepsilon_p^* A_p \left(\sigma T_p^4 - \sigma T_{oc}^4\right) - \varepsilon_\beta A_p \sigma T_p^4 + \varepsilon_\beta A_p q_E + \alpha_\beta A_p \left(q_{s(\,front)} + q_a\right) \tag{32}$$

while the temperature of the outer cover of the MLI covering back of the panel is governed by

$$m_{ocp} c_{ocp} \frac{dT_{ocp}}{dt} = \alpha_{ocp} A_p q_{s(back)} + \varepsilon_p^* A_p \left(\sigma T_p^4 - \sigma T_{ocp}^4\right) - \varepsilon_{ocp} A_p \sigma T_{ocp}^4 - A_{oc4} F_{4-panel} \varepsilon_{oc4} \varepsilon_{ocp} \left(\sigma T_{ocp}^4 - \sigma T_{oc4}^4\right) \tag{33}$$

Now, Equations 28 and 29 for the front longeron and the system of four coupled differential equations (30-33) for the panel and back longeron are solved numerically to determine the temperature of the various truss components throughout the described orbit. Again, steady state temperature responses are plotted.

The model developed in this section allows for a numerical investigation into the thermal response and therefore thermal gradient of the truss with a variety of MLI blankets and outer cover properties. The cases to be considered are shown in Table 2.

Table 2: MLI Blanket Thicknesses and Outer Covers for Numerical Study[8]

Type of MLI and Outer Cover	ε_{tube}^{*}	α/ε	MLI density (kg/m^2)	Outer Cover Density (kg/m^2)	Outer Cover Specific Heat, (J/kg K)
20 layer MLI w/Kapton OC	0.02	0.46/0.81	0.75	0.07	1044
15 layer MLI w/Kapton OC	0.0263	0.46/0.81	0.5625	0.07	1044
10 layer MLI w/Kapton OC	0.038	0.46/0.81	0.375	0.07	1044
5 layer MLI w/Kapton OC	0.07	0.46/0.81	0.1875	0.07	1044
20 layer MLI w/wt.Kapt. OC	0.02	0.2/0.8	0.75	0.17	1009
15 layer MLI w/ wt.Kapt. OC	0.0263	0.2/0.8	0.5625	0.17	1009
10 layer MLI w/ wt.Kapt. OC	0.038	0.2/0.8	0.375	0.17	1009
5 layer MLI w/ wt. Kapt. OC	0.07	0.2/0.8	0.1875	0.17	1009
20 layer MLI w/Ag Tefl. OC	0.02	0.11/0.76	0.75	0.335	1172
15 layer MLI w/Ag Tefl. OC	0.0263	0.11/0.76	0.5625	0.335	1172
10 layer MLI w/Ag Tefl. OC	0.038	0.11/0.76	0.375	0.335	1172
5 layer MLI w/Ag Tefl. OC	0.07	0.11/0.76	0.1875	0.335	1172

Since the radiation exchange between the panel and the back longeron is not significantly affected by the insulation of the back tube, and the white-painted MLI on the radar panel remains the same for the duration of this work, the thermal response of the radar panel and its outer cover is essentially the same as in Figure 9 above. For the first insulated truss case with the longerons covered with MLI blankets with a Kapton outer cover, the thermal response of the front and back longerons is shown in Figure 14 as a function of number of MLI layers. Figures 14-17 below are obtained from the numerical solution of Equations 28-33 with the appropriate properties from Table 2.

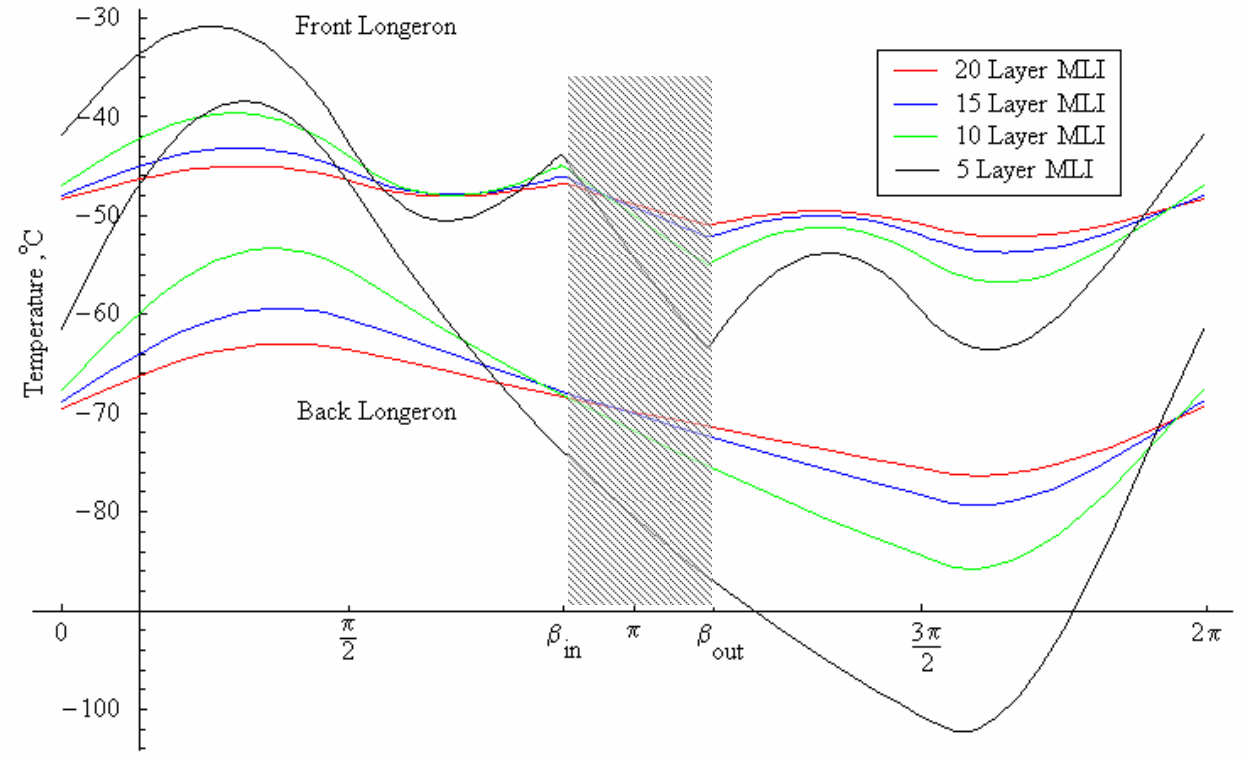

Figure 14: Thermal Response of Truss with MLI and Kapton Outer Cover.

The back longeron is kept warmer by the insulation, while the front longerons are kept cooler, thus lowering the gradient across the truss. This thermal response also shows that increasing the number of layers in the MLI blanket reduces the range of temperatures experienced by the longerons during an orbit. For the next case, the Kapton outer

cover is painted white, thus lowering the solar absorptivity while not significantly changing the surface emissivity. The thermal response of the front and back longerons for this case is shown in Figure 15.

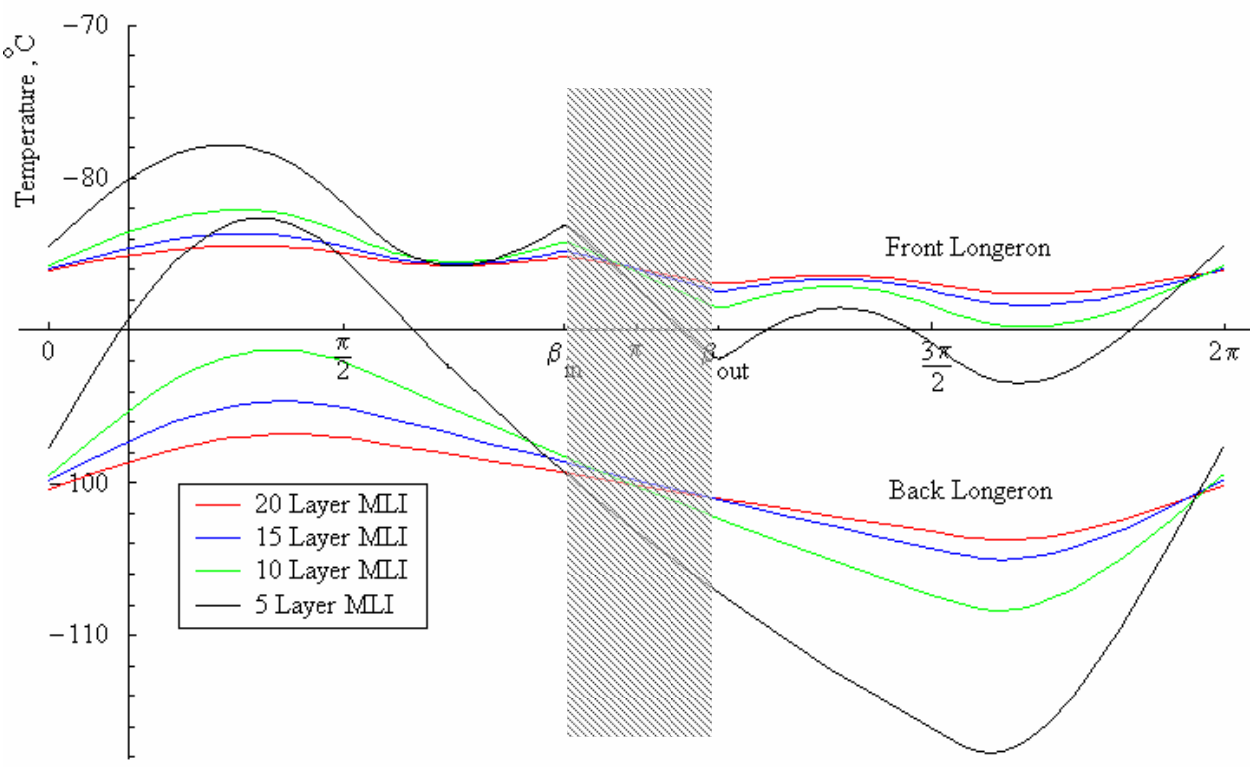

Figure 15: Thermal Response of Truss with MLI and White-Painted Kapton Outer Cover.

As expected, lowering the absorptivity reduces the amount of heat absorbed by the outer cover, and hence, lowers the temperature of the longerons. However, the thermal gradient across the truss appears to be even lower. Once again, the thicker MLI reduces the temperature swings of the truss throughout an orbit, which will lower the change that thermally-induced vibrations will cause a significant structural disturbance. In the last case, the Kapton outer cover is replaced by a thicker, heavier silver-coated Teflon cover. This cover has a very low absorptivity with an emissivity similar to the other outer covers, which, as seen in Figure 15, tends to make the longerons even colder. However, the thermal gradient appears to be even smaller for this case, which requires less truss depth to meet the thermal deformation requirement.

3. Thermal Response Summary for Insulated Truss

In the previous section, the temperature responses of the front and back longerons were predicted independently for a variety of MLI thicknesses and types of outer covers. However, the parameter of interest is the thermal gradient across the truss, that is, the difference between the front and back longerons. For the three insulated cases examined above, Figure 17 shows the calculated thermal gradients across the truss during one orbit. As expected from Figures 14-16, the silver-coated Teflon outer cover produces the smallest thermal gradient, followed by the white-painted Kapton cover, and finally the plain Kapton cover. Even though these insulations result in much lower thermal gradients, they do so because of their reduced solar absorptivity, thus rendering the longerons at low temperatures between approximately -40°C to -120°C. A detailed truss design must ensure that the truss member material performs adequately at these temperatures, and do not suffer any material property degradation, such as increased brittleness, increased modulus or decreased structural damping. In addition, decreasing the number of MLI layers increased the effective emissivity and raised the gradient across the truss. The best performance, exhibited by the 20 or 15 layer MLI blanket with a silver-Teflon outer cover, gave a maximum thermal gradient of around 11°C. It should be noted that the maximum ΔT occurs for all configurations shortly after the truss exits from the shadow of the earth.

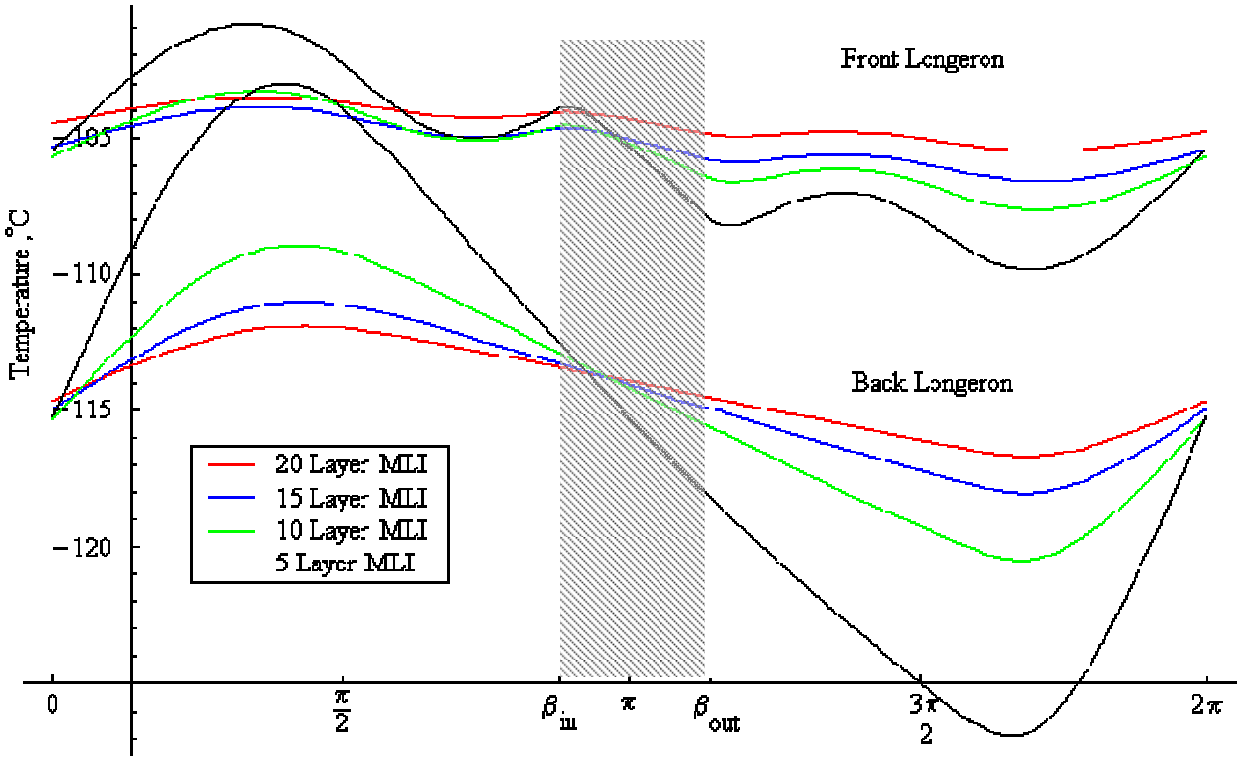

Figure 16: Thermal Response of Truss with MLI and Silver Teflon Outer Cover.

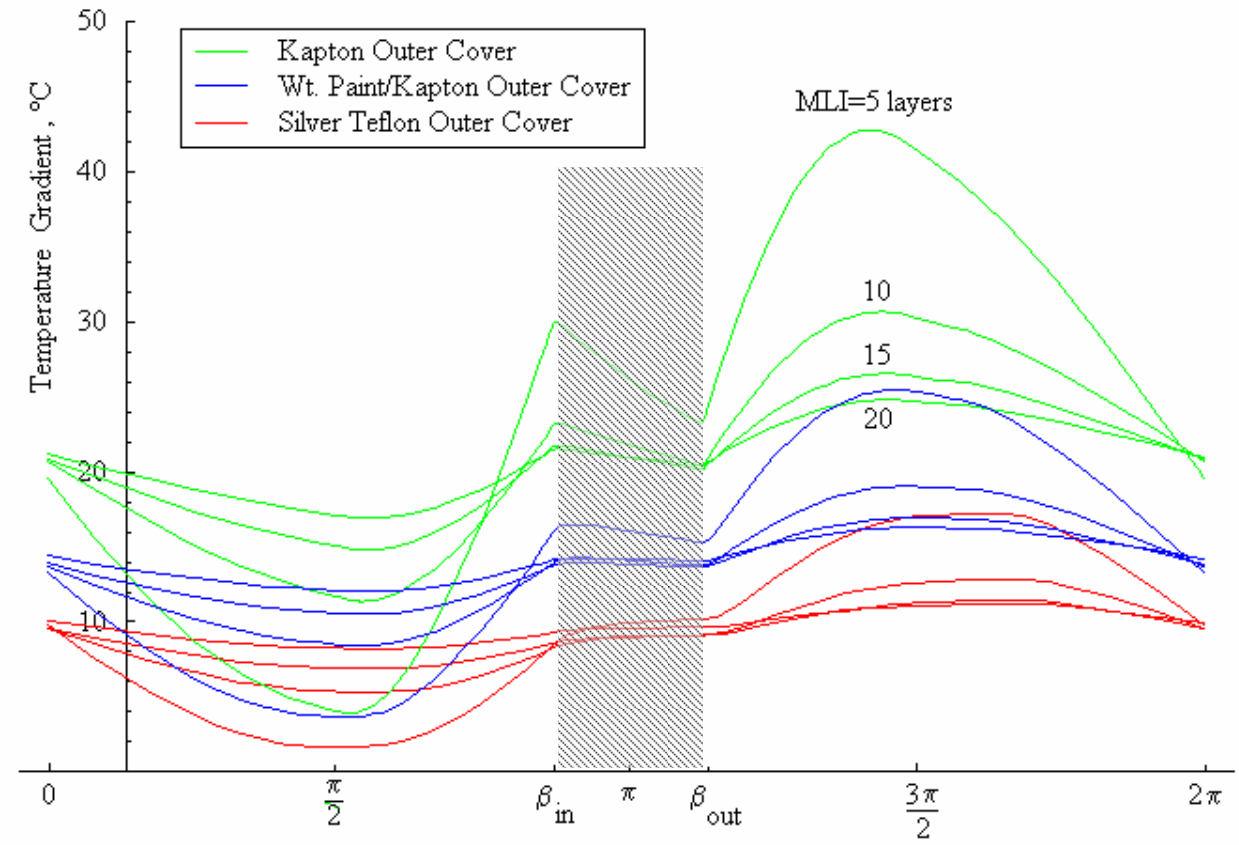

Figure 17: Thermal Gradient across Truss with Various MLI Blankets and Outer Covers.

IV.Results and Mass Estimates for MEO Orbit

Based on the thermal analysis above, the ΔT across the truss has been determined. With the maximum gradients from Figure 17, Equation 8 along is used to determine the truss batten length, *b* (equal to the truss bay length) for the bare truss and the different types of insulation and outer covers. These results are summarized in Table 3.

Table 3: Summary of Results and Mass Estimates for MEO Orbit

Amount of Insulation and Type of Outer Cover	Max ΔT, C	Thermal Req. b (m)	Freq. Req. Dia. (cm)	l/d Req. Dia. (cm)	Max. Req. Dia, (cm)	Bare Truss Mass (kg)	MLI mass (kg)	Outer Cover Mass (kg)	Total Insulated Truss Mass (kg)
Bare Tube	195	23.5	0.01	23.5	23.5	348.9	168.3	0.0	517.2
White paint on bare tube	106	12.7	0.04	12.7	12.7	189.7	92.4	12.2	294.3
20 layer MLI w/Kapton OC	24.75	3.0	0.69	3.0	3.0	44.3	23.2	2.0	69.5
15 layer MLI w/Kapton OC	26.5	3.2	0.60	3.2	3.2	47.4	24.7	2.1	74.3
10 layer MLI w/Kapton OC	30.5	3.7	0.45	3.7	3.7	54.6	28.1	2.5	85.2
5 layer MLI w/Kapton OC	42.75	5.1	0.23	5.1	5.1	76.5	38.5	3.5	118.5
20 layer MLI w/wt.Kapt. OC	16	1.9	1.65	1.9	1.9	28.6	15.8	3.1	47.5
15 layer MLI w/ wt.Kapt. OC	16.75	2.0	1.51	2.0	2.0	30.0	16.4	3.3	49.6
10 layer MLI w/ wt.Kapt. OC	19	2.3	1.17	2.3	2.3	34.0	18.3	3.7	56.0
5 layer MLI w/ wt. Kapt. OC	25.5	3.1	0.65	3.1	3.1	45.6	23.9	5.0	74.4
20 layer MLI w/Ag Tefl. OC	10.75	1.3	3.66	1.3	3.7	54.4	28.0	11.6	94.0
15 layer MLI w/Ag Tefl. OC	11	1.3	3.49	1.3	3.5	51.9	26.9	11.1	89.9
10 layer MLI w/Ag Tefl. OC	12.5	1.5	2.70	1.5	2.7	40.2	21.3	8.6	70.1
5 layer MLI w/Ag Tefl. OC	17.1	2.1	1.45	2.1	2.1	30.6	16.7	6.5	53.8

For these batten lengths determined from thermal distortion requirements, the diameter of the longerons can be determined using both slenderness (Equation (6)) and frequency (Equation (7)) requirements. The larger of these two diameters must be selected to ensure that both slenderness and frequency requirements are met simultaneously. For the calculated gradients, all of the longeron diameters are dominated by the slenderness ratio except for the three thickest MLI blankets with silver-Teflon outer covers, which are frequency-driven. With the geometry of the truss now fully prescribed by thermal and structural requirements, Equations 9 and 10 are used to estimate the mass of the truss, the MLI insulation mass, and the mass of the outer cover. The right-most column of Table 3 shows the total insulated truss mass that meets all of the given requirements. The minimum mass truss is for the 20 layer MLI blanket with white-painted Kapton outer cover. However, it is interesting to note that this configuration does not have the lowest thermal gradient. It turns out that the silver-Teflon outer covers reduce the thermal gradient so low that the truss becomes *too* shallow, and therefore the longerons must increase in diameter a great deal in order to meet the frequency requirements. These frequency-driven, large diameter longerons result in a truss that weighs almost twice as much as one that is slenderness-driven with a slightly higher thermal gradient.

V. Results and Mass Estimates for LEO and GEO Orbits

While the thermal model developed above considered a MEO orbit, it is readily adapted to account for an equatorial circular orbit of any altitude. Two common orbits of interest are low-earth orbit (LEO) and geostationary orbit (GEO), taken to be at 279 km and 35,875 km, respectively. While a complete investigation into the results for these two orbits is beyond the scope of this project, a summarized version is provided in Tables 4 and 5, which are obtained from numerical solution of Equations 28-33 with the appropriate material properties from Table 2 and the respective orbital altitude. Many important trends are noted from Tables 3-5 for the three orbital altitudes. First, higher orbits result in higher gradients and thus heavier trusses for the uninsulated longeron cases. Also, at LEO, additional layers of MLI do not significantly affect the thermal gradient or the total insulated truss mass. However, at the two higher orbits, additional MLI layers significantly decrease the thermal gradient. Trusses in LEO tend to have the highest insulated mass except if minimal MLI blanketing is used. As for meeting the structural requirements, each of the LEO truss designs are slenderness dominated, which is indicative of larger thermal gradients requiring deeper trusses. At GEO, only the highest level of insulation reduces the thermal gradient to the point that the design becomes driven by frequency requirements.

Table 4: Summary of Results and Mass Estimates for LEO Orbit

Amount of Insulation and Type of Outer Cover	Max ΔT, C	Thermal Req. b (m)	Freq. Req. Dia. (cm)	l/d Req. Dia. (cm)	Max. Req. Dia, (cm)	Bare Truss Mass (kg)	MLI mass (kg)	Outer Cover Mass (kg)	Total Insulated Truss Mass (kg)
Bare Tube	75.1	9.0	0.07	9.0	9.0	134.4	0.0	0.0	134.4
White paint on bare tube	68.5	8.2	0.09	8.2	8.2	122.6	0.0	7.9	130.5
20 layer MLI w/Kapton OC	31.9	3.8	0.42	3.8	3.8	57.1	29.3	2.6	89.0
15 layer MLI w/Kapton OC	32	3.8	0.41	3.8	3.8	57.3	29.4	2.6	89.2
10 layer MLI w/Kapton OC	32.4	3.9	0.40	3.9	3.9	58.0	29.7	2.6	90.3
5 layer MLI w/Kapton OC	33.4	4.0	0.38	4.0	4.0	59.8	30.6	2.7	93.0
20 layer MLI w/wt.Kapt. OC	38	4.6	0.29	4.6	4.6	68.0	34.5	7.4	109.9
15 layer MLI w/ wt.Kapt. OC	38	4.6	0.29	4.6	4.6	68.0	34.5	7.4	109.9
10 layer MLI w/ wt.Kapt. OC	38.2	4.6	0.29	4.6	4.6	68.3	34.7	7.4	110.4
5 layer MLI w/ wt. Kapt. OC	38.9	4.7	0.28	4.7	4.7	69.6	35.3	7.6	112.4
20 layer MLI w/Ag Tefl. OC	42.6	5.1	0.23	5.1	5.1	76.2	38.4	16.3	130.9
15 layer MLI w/Ag Tefl. OC	42.7	5.1	0.23	5.1	5.1	76.4	38.5	16.3	131.2
10 layer MLI w/Ag Tefl. OC	42.9	5.2	0.23	5.2	5.2	76.8	38.7	16.4	131.8
5 layer MLI w/Ag Tefl. OC	43.6	5.2	0.22	5.2	5.2	78.0	39.3	16.6	133.9

Table 5: Summary of Results and Mass Estimates for GEO Orbit

Amount of Insulation and Type of Outer Cover	Max ΔT, C	Thermal Req. b (m)	Freq. Req. Dia. (cm)	l/d Req. Dia. (cm)	Max. Req. Dia, (cm)	Bare Truss Mass (kg)	MLI mass (kg)	Outer Cover Mass (kg)	Total Insulated Truss Mass (kg)
Bare Tube	236.8	28.5	0.01	28.5	28.5	423.7	0.0	0.0	423.7
White paint on bare tube	143.5	17.3	0.02	17.3	17.3	256.8	0.0	16.5	273.3
20 layer MLI w/Kapton OC	47	5.7	0.19	5.7	5.7	84.1	42.2	3.8	130.1
15 layer MLI w/Kapton OC	58.2	7.0	0.12	7.0	7.0	104.1	51.7	4.7	160.6
10 layer MLI w/Kapton OC	77	9.3	0.07	9.3	9.3	137.8	67.7	6.2	211.7
5 layer MLI w/Kapton OC	109	13.1	0.04	13.1	13.1	195.0	95.0	8.8	298.9
20 layer MLI w/wt.Kapt. OC	24.4	2.9	0.71	2.9	2.9	43.7	22.9	4.7	71.3
15 layer MLI w/ wt.Kapt. OC	30.5	3.7	0.45	3.7	3.7	54.6	28.1	5.9	88.6
10 layer MLI w/ wt.Kapt. OC	41.9	5.0	0.24	5.0	5.0	75.0	37.8	8.1	120.9
5 layer MLI w/ wt. Kapt. OC	66.2	8.0	0.10	8.0	8.0	118.4	58.5	12.9	189.8
20 layer MLI w/Ag Tefl. OC	12.4	1.5	2.75	1.5	2.7	40.9	21.6	8.7	71.2
15 layer MLI w/Ag Tefl. OC	16.6	2.0	1.53	2.0	2.0	29.7	16.3	6.3	52.3
10 layer MLI w/Ag Tefl. OC	24.7	3.0	0.69	3.0	3.0	44.2	23.2	9.4	76.8
5 layer MLI w/Ag Tefl. OC	43.6	5.2	0.22	5.2	5.2	78.0	39.3	16.6	133.9

VI.Conclusion

This work was to develop a simple transient radiation heat transfer model for a long, linear, triangular truss that supports a radar panel in MEO orbit that does not require special thermal analysis software. The results of this thermal model were used along with previously investigated structural requirements to size the truss and estimate its mass, along with the mass of the MLI blankets and outer covers. The results show that a bare graphite-epoxy or white-painted truss would be much too large and weigh too much to meet these requirements. The addition of MLI blankets with various types of outer covers greatly reduced the thermal gradient across the truss and hence resulted in a much lower insulated truss mass. However, there exists a point when the thermal gradient becomes so small that the truss becomes too shallow and the longerons must become quite large in order to meet the frequency requirements. Thus, an important trade between structural requirements and thermal response has been identified. Additionally, the thermal response of the truss to LEO and GEO orbital altitudes was predicted. It was found that additional layers of MLI are not effective at LEO in reducing thermal gradients or insulated system mass, while they work increasingly well at higher orbits. In addition, all of the LEO and all buy one of the GEO truss designs are slenderness dominated, which is indicative of larger thermal gradients requiring deeper, more massive trusses.

Acknowledgments

The Innovative Space Antenna Technology (ISAT) program at NASA Jet Propulsion Laboratory provided the financial support to perform the work presented in this paper. The research described in this paper was carried out at the Jet Propulsion Laboratory, California Institute of Technology, under a contract with the National Aeronautics and Space Administration.

References

[1]Mikulas, M. M., Jr., "Structural Efficiency of Long Lightly Loaded Truss and Isogrid Columns for Space Applications," NASA TM-78687, 1978.

[2]Mikulas, M. M., Jr, "ISAT Truss Design Considerations," *Powerpoint Presentation to the ISAT Design Team*, Unpublished, 2003.

[3]Mahaney, J., and Strode, K. B., "Fundamental Studies of Thermal-Structural Effects on Orbiting Trusses," AIAA-1982-0650, *Proceedings of the 23rd Structures, Structural Dynamics, and Materials Conference*, New Orleans, LA, May 1982, pp. 49-59.

[4]Cunningham, F. G., "Power Input to a Small Flat Plate from a Diffusely Radiating Sphere, with Application to Earth Satellites," NASA TN D-710, August 1961.

[5]Modest, M. F., "Solar Flux Incident on an Orbiting Surface after Reflection from a Planet," *AIAA Journal*, Vol 18, No. 6, pp. 727-730.

[6]Karam, R. D., *Satellite Thermal Control for Systems Engineers*, Progress in Astronaurics and Aeronautics, Volume 181, American Institute of Aeronautics and Astronautics, Inc., 1998

[7]Gilmore, D. G., Editor, "Spacecraft Thermal Control Handbook, Volume I: Fundamental Technologies," The Aerospace Press, El Segundo, CA, 2002.

[8]Wertz, J. R., and Larson, W. J., *Space Mission Analysis and Design*, Microcosm Press, Los Angeles, 1999, Chap. 11.

[9]Williams, R. B., and Agnes, G. S., "Mass Efficiencies for Common Large-Scale Precision Space Structures, AIAA-2005-2050, *Proceedings of the 46th Structures, Structural Dynamics, and Materials Conference*, Austin, TX, April 2005.